Sensors & Actuators: B. Chemical 422 (2025) 136617

Contents lists available at ScienceDirect

Sensors and Actuators: B. Chemical

journal homepage: www.elsevier.com/locate/snb

Flexible droplet microfluidic devices for tuneable droplet generation

Uditha Roshan [a], Yuchen Dai [b], Ajeet Singh Yadav [a], Samith Hettiarachchi [a], Amith Mudugamuwa [a], Jun Zhang [a,c,*], Nam-Trung Nguyen [a,**]

[a] Queensland Micro and Nanotechnology Centre, Griffith University, Nathan, QLD 4111, Australia
[b] School of Chemical Engineering, The University of Queensland, Brisbane, QLD 4072, Australia
[c] School of Engineering and Built Environment, Griffith University, Nathan, QLD 4111, Australia

ARTICLE INFO

Keywords:
Flexible and stretchable microdroplet formation
Flexible microfluidics
Micro elastofluidics
Droplet microfluidics

ABSTRACT

Droplet microfluidics is a promising technology for applications that require precise handling of minute fluid volumes. This technology has broad applications in the pharmaceutical industry, food and beverage, and material synthesis. Droplet size and frequency are the two key parameters in these applications. Current droplet microfluidic devices are rigid platforms where the geometry and dimensions of microchannels are fixed after the device fabrication. This poses a significant limitation when adjusting the droplet generation characteristics. Repetitive design, fabrication, and testing are often needed to achieve the optimal microchannel dimensions. To overcome this bottleneck, we develop a proof-of-concept stretchable microfluidic device that can control droplet size and generation frequency by precisely controlling the microchannel dimensions in real-time. Theoretical analysis, numerical modelling, and experimental characterisation were conducted to study the influence of device lateral stretching on these characteristics. We found that the lateral stretching of the device increased the droplet diameter and spacing but reduced the droplet generation frequency. Droplet diameter and spacing increased by ~20 %, and droplet frequency decreased by ~45 % when the device was strained up to 25 %. We believe this innovative, flexible droplet microfluidic platform will provide an alternative way to precisely control the droplet formation by modifying the channel dimensions on-site and in real-time.

1. Introduction

Droplet microfluidics generates, manipulates, and controls sub-microlitre fluid volumes or droplets dispersed in an immiscible fluid stream [1–4]. These droplets have broad applications in the pharmaceutical industry [5], food and beverage [6], single-cell analysis [7], material synthesis [8], high-throughput molecular genetics [9], emulsification and particle synthesis [10]. For instance, encapsulating individual circulating tumour cells (CTCs) in monodispersed droplets is essential for single-cell analysis for cancer diagnosis and personalised medicine [1]. The volume of microdroplets created by this technology ranges from nanoliter to picolitre, resulting in reduced sample and reagent consumption compared to traditional single-cell analysis techniques. In addition, droplet monodispersity ensures reproducibility and consistency in material synthesis and analysis. Importantly, altering the droplet sizes in real time would offer versatility and optimisation potential for various applications that require a range of droplet volumes. The flexibility to change droplet size makes the system adaptable. Droplet microfluidics is also widely used in pharmaceutical research and drug discovery by simultaneous high-throughput screening of thousands of drug candidates in droplets, significantly accelerating the drug discovery process [11]. Therefore, the success of these applications depends on the robust, efficient, and flexible generation of a large number of droplets with desired properties such as droplet size, spacing, and frequency.

Droplet generation can be achieved by active and passive microfluidic methods [12–15]. Passive methods depend on the microchannel geometry and the flow characteristics of the liquid phases involved in droplet formation. Droplet generation happens through instabilities in the flow field. [16] Active methods utilise additional energy input by external active sources such as electric, magnetic, thermal, and acoustic fields to form droplets [17]. Passive droplet generation possesses the advantages of simplicity and cost-effectiveness, scalability, and ease of microfabrication [17]. In a passive method, droplets are generated when

* Corresponding author at: Queensland Micro and Nanotechnology Centre, Griffith University, Nathan, QLD 4111, Australia
** Corresponding author.
E-mail addresses: jun.zhang@griffith.edu.au (J. Zhang), nam-trung.nguyen@griffith.edu.au (N.-T. Nguyen).

https://doi.org/10.1016/j.snb.2024.136617
Received 24 April 2024; Received in revised form 19 August 2024; Accepted 8 September 2024
Available online 10 September 2024

the forces caused by the pressure gradient across the droplet and the shear force on the droplet interface overcome the interfacial tension force. The shear force results from the velocity mismatch of the continuous and the dispersed phases, while the interfacial tension resists the droplet breakup [18]. Thus, passive droplet generation highly depends on the flow rates of continuous and dispersed fluid phases. The channel configuration also plays a vital role in passive droplet generation. Common channel configurations include the crossflow (T-junction, Y-junction),[19,20] co-flow [21], and flow-focusing [22] arrangements. Other geometries, such as step emulsification and membrane structures, have also been reported [23,24]. Among these configurations, the flow-focusing design is simple and has the advantages of precise control of droplet size, high throughput, and low shear stress associated with droplet breakup [25].

Extensive research has been carried out with numerical modelling and experimental approaches to improve the droplet generation process and to obtain desired droplet characteristics [22,26]. These works investigated the geometrical parameters of microfluidic channel structures, such as the entry angle of the continuous phase [27], the intersection angles of the two phases [28], constriction width and length [29], etc. However, these works are primarily based on rigid microfluidic devices. The channel geometry and dimension cannot be adjusted after device fabrication. A summary of these works can be found in Supplementary Information S-4, Table S1. Apart from these previous works, very few studies have explored ways to modify channel dimensions to control droplet generation actively. Lee et al. [30] studied active flow-focusing microdroplet generation using controllable moving walls. Pneumatically actuated side chambers were placed next to the flow channel to adjust its width. Upon applying pneumatic pressure, the fluid stream width could be reduced from 30 to 9 μm, resulting in the generation of droplets with a diameter of 76 μm.

Moreover, Nalin et al. [31] recently reported a tuneable droplet generation device based on step emulsification. Here, a pneumatically actuated membrane was placed under the step nozzle. The height of the nozzle was reduced by applying pressure to obtain three orders of magnitude variation in droplet size without adjusting the flow rates of the two phases. The applied pressure reduced the generated water-in-oil droplet diameter from 551 μm to 64 μm. These works highlighted the ability to move channel walls pneumatically for tuning droplet generation. In addition, Yazdanparast et al. [32] conducted a similar study by squeezing a co-flow channel to change the continuous phase velocity. Here, two moving blocks squeezed the continuous phase channel wall around the dispersed phase needle and adjusted the continuous phase flow velocity. Squeezing the 1-mm channel width down to 0.3 mm altered the droplet diameter from 913 μm to 175 μm. Furthermore, Abate et al. [33] presented a valve-based flow-focusing droplet formation concept where pressurised water acted on membrane valves to control the constriction width. Reducing the constriction width changed the droplet diameter from 200 μm to 7 μm. However, all these works only considered the deformation of only part of the microchannel structure. Additional channel networks had to be considered to facilitate the control layers, making size-tuneable droplet generators somewhat complex.

In the present work, we developed a fully flexible and stretchable microfluidic technology [34,35] for tuneable droplet generation. We chose to stretch the entire microfluidic device, which presents adaptability and simplicity in prospective application areas compared to previous works discussed. We have selected stretching as the actuation method among the various techniques for actuating flexible and stretchable microdevices to change the microchannel dimensions within the flexible device [36]. The channel dimensions of the proposed flexible device can be changed accurately in real-time by external stretching so that droplet generation characteristics, such as droplet size, droplet space, and generation frequency, can be precisely tuned. We selected the flow-focusing configuration to test the above hypothesis. First, theoretical analysis and numerical modelling were used to investigate the effect of change in channel dimensions on droplet generation. Next, we developed the flexible and stretchable droplet microfluidic device and evaluated the variation of channel dimensions under various stretching conditions. Subsequently, we experimentally studied the effects of device stretching on droplet generation characteristics under different flow rates. The results showed that stretching the device can increase the droplet diameter and spacing and decrease the droplet frequency. Droplet diameter and spacing increased by ~20 %, and droplet frequency decreased by ~45 % when the device was strained up to 25 %. We believe this flexible and stretchable droplet microfluidic technology offers a promising new way to generate tunable droplets by controlling the channel dimensions on-site and in real-time.

2. Theoretical analysis

The droplet formation process in a microfluidic device can be explained by the Plateau-Rayleigh instability phenomenon [37]. The capillary instability under the effect of inertial and viscous forces forms a droplet. The interfacial tension at the fluid interface stabilises the shape of the droplet [38]. The droplet formation in a microfluidic channel exhibits regimes such as squeezing [39], dripping, jetting [40], tip-streaming [41], and tip-multi-breaking [42], depending on the flow characteristics, such as flow rate and fluid properties such as density, viscosity, as well as the channel geometry. Our present work uses a flow-focusing microfluidic channel geometry to generate droplets in the dripping regime. The produced droplets are highly monodispersed and spherical in the dripping regime. Several studies have shown the significance of channel geometry on droplet formation in flow-focusing, T-junction, and co-flow configurations [43–46]. Stretching the droplet generator device is a novel and simple method of changing critical channel dimensions, facilitating the formation of size-tuneable droplets with different formation frequencies, Fig. 1(a). The supplementary information S-1 provides a more fundamental description of the effect of stretching on droplet formation.

However, droplet plug length (L_{plug}), Fig. 1(b). is one of the parameters that can be used to quantify the regimes of droplet formation and characteristics of generated droplets [46]. The plug length of monodispersed spherical droplets generated in the dripping regime is equivalent to the droplet diameter. The following theoretical analysis was conducted to quantify the effect of dimensional changes on the droplet plug length and generation frequency.

The generated droplet plug length can be predicted by the power law [46]:

$$\frac{L_{plug}}{w_c} = (\widetilde{\varepsilon} + \widetilde{\omega} Q) Ca^{\widetilde{m}} \tag{1}$$

where $\widetilde{\varepsilon}$, $\widetilde{\omega}$, $\widetilde{m}$ are fitting coefficients which mainly depend on the channel geometry parameters such as channel depth (H) and widths (w). Here, w_c and Ca is the continuous phase channel width and the capillary number. $\widetilde{\varepsilon}$ and $\widetilde{\omega}$ are positive values and increase with the dispersed phase channel width, while $\widetilde{m}$ is a negative value (around −0.3) [46].

By stretching the PDMS device, which has a Poisson ratio of about 0.5 [47], so that,

$$\frac{\Delta w_c}{w_c} = \frac{\Delta H}{H} = \left(1 + \frac{\Delta w_{cw}}{w_{cw}}\right)^{-0.5} - 1 \tag{2}$$

where $\frac{\Delta w_{cw}}{w_{cw}}$ is the input stretching ratio. w_{cw} is the constriction width. Let $1 + \frac{\Delta w_{cw}}{w_{cw}} = \alpha$ be the stretching variable, it is easy to obtain:

$$w_c + \Delta w_c = w_c \alpha^{-0.5} \tag{3}$$

$$H + \Delta H = H \alpha^{-0.5} \tag{4}$$

Correspondingly, the capillary number Ca is affected by the stretching variable α as:

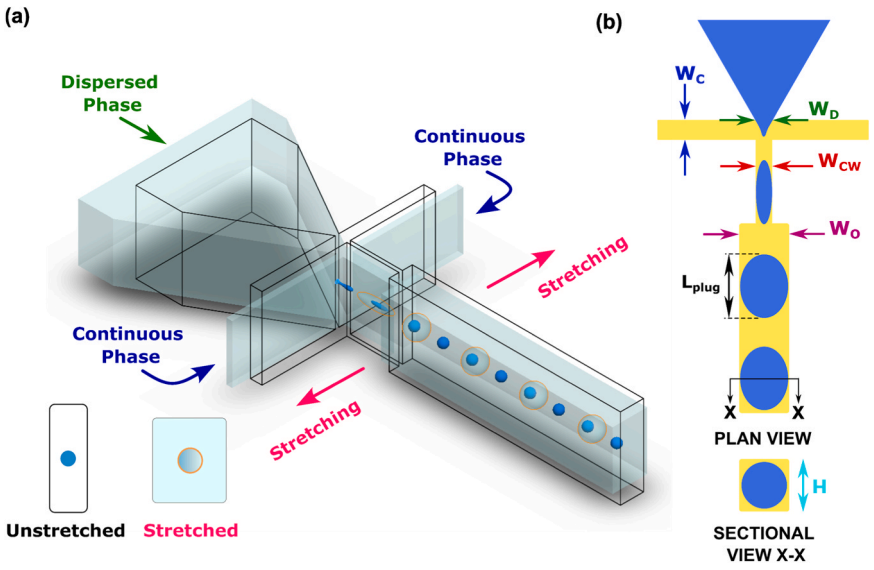

Fig. 1. Schematic of change of channel dimensions and droplet generation by stretching the device. (a) Change of channel geometry and droplet characteristics upon stretching. (b) Parameters considered for theoretical analysis.

$$Ca = \frac{\eta U}{\gamma} = \frac{\eta Q_c}{\gamma(w_c + \Delta w_c)(H + \Delta H)} = \frac{\eta Q_c}{\gamma} \bullet \frac{\alpha}{w_c H} \tag{5}$$

Here, η, γ, and U are the dynamic viscosity, surface tension, and the characteristic velocity of the fluid flow. As observed, the capillary number is linearly proportional to the stretching variable α. Substituting **(5)** into **(1)**, assuming the flow rate Q is constant, the droplet size (D_d) relates with the stretching variable α as:

$$\frac{D_d}{w_c} = \frac{L_{plug}}{w_c} = k\alpha^m \tag{6}$$

Here k and m are the scaling law coefficients for droplet size. The droplet generation frequency (f) is the inverse of pinch-off time (t_p), which can be estimated as:

$$t_p = \frac{V_d}{Q_d} \tag{7}$$

Although the shape of the droplets have an upper and a lower flat surface in the expansion section, i.e., w_{cw} as the width, the droplet volume V_d should still be scaled by the spherical volume formula:

$$V_d \sim \frac{4\pi}{3}\left(\frac{D_d}{2}\right)^3 \tag{8}$$

Substituting **(8)** and **(6)** into **(7)** results in the droplet pinch-off time as a function of stretching variable α as:

$$t_p = k'\alpha^{m'} \tag{9}$$

where k' and m' are the scaling law coefficients related to the droplet pinch-off time. And k' is estimated about 100 times smaller than k while m' is around three times of m.

Eqs. (6) and (9) indicate that the droplet size and generation frequency are sensitive to the device strain. If the value of m or m' is positive, stretching the device along the lateral direction will increase the droplet size and decrease the generation frequency. In contrast, if the value of m and m' is negative, elongating the device along the lateral direction will reduce the droplet size and enhance generation frequency. We can also estimate the value of m and k (or m', k') by fitting experimental data with the exponential function.

3. Materials and methods

3.1. Device design and fabrication

The master mould used to fabricate the microchannel layer (Fig. 2 (a)) of the flexible droplet generator device was previously designed and introduced by Teo et al. [48]. Galogahi et al. [12] later utilised this design to form UV-curable core-shell microcapsules for applications such as the storage and delivery of oil-based materials in skin care products or reagents for biochemical assays. Therefore, we utilised this proven microchannel design to evaluate the effect of device stretching on droplet formation. The additional features available in the previous design for the infusion of the spacer fluid were not needed in the present study. The flow-focusing device used in our experiments has two inlets for continuous (C-Phase) and dispersed (D-Phase) fluid phases, respectively, and an outlet (Fig. 2(a)). The symmetrical C-Phase channels meet the D-Phase orifice at 90°. The initial widths of the C-Phase channel and D-Phase orifice are 40 μm and 63 μm, respectively. After the junction where the fluid meets, there is a constriction with a width of 29 μm and a length of ~412 μm, facilitating the hydrodynamic focusing of the two fluids. Downstream, the constriction is the droplet outlet channel with a 90-μm width, which extends until the outlet. All channel sections have a constant height of ~137 μm.

The flow-focusing microfluidic device was fabricated using the standard photolithography and soft lithography techniques [49]. SU-8 3050 negative photoresist material from MicroChem Corp. was used to develop the mould on silicon wafers through standard photolithography. Here, polydimethylsiloxane (PDMS) (Sylgard 184, Dow Corning) prepolymer thoroughly mixed with curing agent at a 10:1 ratio was degassed and poured onto the SU-8 mould. The amount of polymer mixture was selected to achieve a ~500 μm thin PDMS channel layer. The mould was then kept in a properly levelled oven at 75°C for ~2 hours to allow PDMS to solidify. Then, the solidified PDMS channel layer was carefully peeled off. Subsequently, a thin PDMS channel enclosing layer (~500 μm) was bonded to the channel layer. Two thick PDMS blocks (~5 mm) were bonded onto the top of the channel layer to facilitate the inlets and outlet tubing connection. Finally, two PDMS clamping supporting slabs (~6 mm) and two PDMS clamping supporting layers (~1 mm) were bonded along both sides of microchannels on top and bottom of thin PDMS layers (Fig. 2(a)), respectively. All the PDMS-to-PDMS bonding was performed with plasma treatment. The fabrication process was explained in detail in our previous work

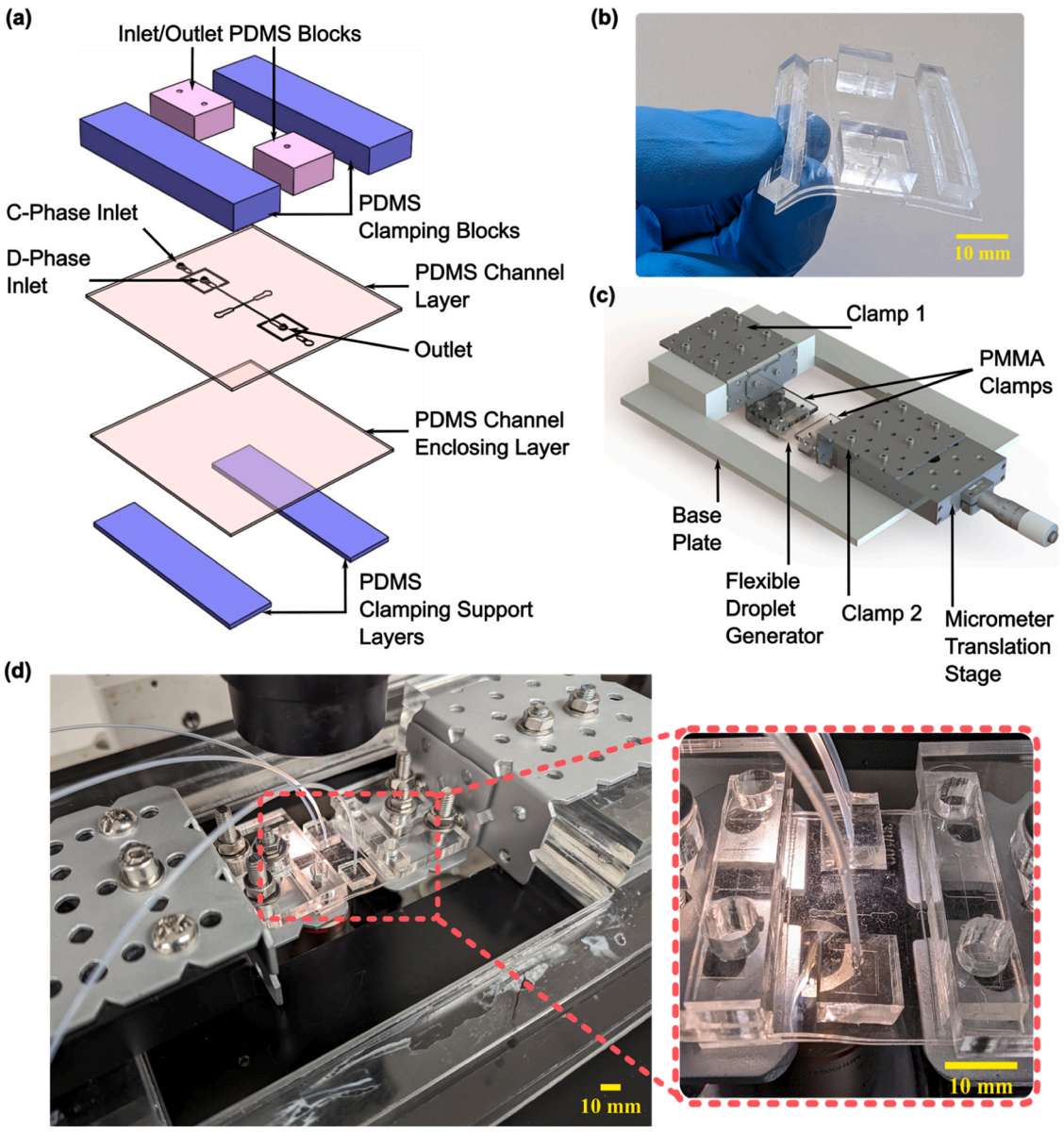

Fig. 2. (a) Schematic configuration of the stretchable droplet microfluidic device. (b) A photograph of a fabricated flexible droplet microfluidic device. (c) Schematic illustration of the stretching platform and the flexible droplet device. (d) A photograph of the experimental setup. The enlarged image shows the flexible droplet microfluidic device under elongation.

[50–52].

3.2. Discrete and continuous fluid phases

Using the developed flexible flow-focusing microdroplet generator device Fig. 2(b), droplets of fluorinated oil (HFE, Novec 7500 3 M) were generated using trimethylolpropane trimethacrylate (TMPTMA, Sigma-Aldrich Co.) as the continuous phase. Here, the HFE 7500 and TMPTMA liquids were chosen to generate HFE 7500 monodispersed droplets [48, 53]. In addition, TMPTMA has good chemical compatibility and high thermal stability [54] when it comes to possible application areas [48]. The liquid properties at 25 °C are given in Table 1.

3.3. Experimental setup

The experimental setup consists of a stretching platform [52], Fig. 2

Table 1
Properties of continuous and dispersed phases.

Medium	Type	Density (g/cm^3)	Dynamic viscosity ($mPa.s$)	Surface tension (mN/m)	Interfacial tension (mN/m)
Continuous Phase (C-Phase)	Trimethylolpropane trimethacrylate (TMPTMA)	1.06	42	32.5	3.45 [53,55]
Dispersed Phase (D- Phase)	Hydrofluoroether 7500 (HFE 7500)	1.63	1.31	15.52	

(c), an optical microscope with a high-speed camera, and two syringe pumps. The stretching platform is composed of a micrometre translation stage on top of a PMMA base plate. Two metal clamps were attached to the base plate, and the translation stage was used to facilitate device clamping. Two PMMA slabs were used to fix the flexible PDMS micro-droplet generator in between the metal clamps. After clamping, the translational stage was adjusted to make the flexible device recover initial deformations before experiments. The initial channel lengths were measured as a reference while adjusting the translation stage to ensure the device was precisely stretched.

The stretching platform with the PDMS device was placed on the stage of an inverted microscope (Olympus, IX73), Fig. 2(d). Two syringe pumps (DK INFUSETEK ISPLab02) precisely controlled the flow rates of the continuous and dispersed phase flows into the microfluidic device. A high-speed CCD camera (Phantom, Vision Research) was mounted on the microscope and recorded videos of the droplets at the outlet using an exposure time of 30 μs. The videos recorded were analysed using Droplet Morphometry and Velocimetry (DMV) software [56] and extracted quantitative information on the size, spacing, and frequency of the droplets. Besides, the open-source ImageJ (National Institutes of Health USA) software was used to measure the channel dimensions under device stretching.

3.4. Experimental procedure

Experiments were conducted for five elongations (1–5 mm) by tuning the micrometre translation stage. The following tests were carried out to evaluate the effect of stretching on the dimensions of channels, droplet diameter, spacing, and droplet generation frequency: (i) Stretching and stretch releasing test to evaluate the change of the microchannel dimensions; (ii) Constant total flow rate test – the device was stretched from 0 to 5 mm by 1 mm steps while keeping the total flow rate (Q_c+Q_d =) at 120 μL/hr. The flow rate ratio (Q_c/Q_d) varies from 1–5; (iii) constant flow rate ratio test – the device was stretched from 0 to 5 mm by 1 mm steps while keeping the flow rate ratio (Q_c/Q_d = 2) with the total flow rates ranging from 90 to 180 μL/hr. All stretching experiments were conducted three times. A maximum elongation of 5 mm was selected to make sure that PDMS was in its elastic range during stretch-release cycles [57]. For 5-mm elongation, the flexible PDMS device was laterally strained to 25 %, which is still in the elastic region.

After stretching the device with each 1-mm step, videos were captured after allowing the flexible device to stabilise and produce a uniform stream of droplets. Videos were recorded 1 minute after stretching. Each video has on average 200 frames. Each frame contains 10 – 15 droplets depending on the elongation of the microfluidic device. The diameter of each droplet and spacing between each consecutive droplets were measured throughout the duration of the video. The mean and standard deviation of the population were calculated to represent droplet characteristics of a particular stretching scenario.

4. Results and discussion

4.1. Microfluidic channel deformation under device stretching

We investigated the dimensional change of the microchannels under various elongations using numerical modelling and experiments. The geometry and dimensions of the microchannel arrangement in Fig. 1(b) were considered in this study. The initial dimensions of the flow-focusing microchannel before stretching are the width of the dispersed

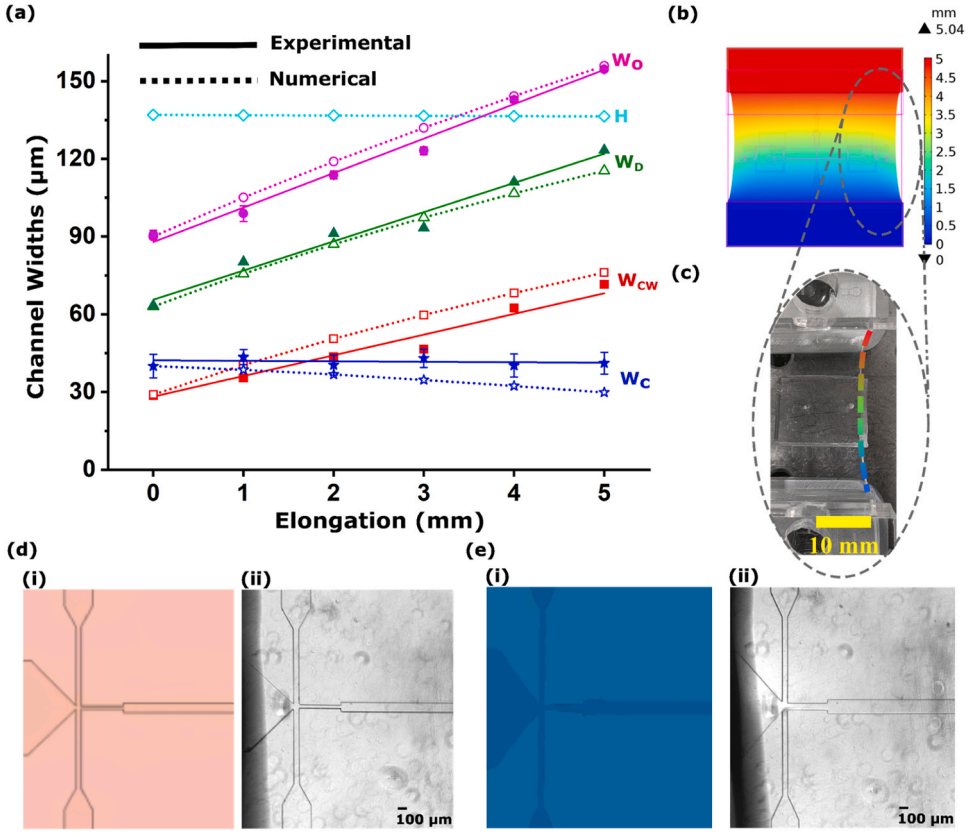

Fig. 3. Dimensional changes of the microfluidic device of flow-focusing geometry under lateral stretching. (a) Experimentally measured and numerically simulated microchannel dimensions under various device elongations. (b) Simulated deformation of the microfluidic device under 5-mm device stretching. The colour bar indicates displacement. (c) The deformed microfluidic device under 5-mm device stretching. (d) Flow-focusing microchannel arrangement before stretching. (e) after 5-mm stretch. (i) geometry in the simulation environment, (ii) microscopic image.

phase inlet (W_D) 63 μm, constriction (W_{CW}) 29 μm, droplet outlet channel (W_O) 90 μm, the height of the channel (H) 137 μm, and the continuous phase channel width (W_C) 40 μm. The device was elongated laterally, perpendicularly to the flow direction, ranging from 0 to 5 mm by 1-mm steps, Fig. 1(a). The variation of channel widths and height was evaluated at different elongation distances. Fig. 3(a) shows the data of experimental measurement and numerical simulation of microchannel dimensions with respect to device elongation. The numerical analysis of the channel deformation was conducted using COMSOL Multiphysics 5.4. Solid mechanics physics interface was used to evaluate the device deformation. A physics-controlled mesh was created to capture the device deformation accurately, and a stationary study was used to compute the model. More details about the simulation model can be found in Supplementary information S-2. As expected, increasing the elongation increases the width of the dispersed phase inlet (W_D), constriction (W_{CW}), and droplet outlet channel (W_O). In contrast, the height of the channel (H), and the continuous phase channel width (W_C) were reduced when increasing the elongation. Fig. 3(b) illustrates the simulated deformation of the microfluidic device under 5-mm elongation, and Fig. 3(c) shows the deformed microfluidic device under the same stretching condition in the experiments. Fig. 3(d) and (e) show the simulated and actual microscopic images of microchannel geometry after and before stretching.

4.2. Numerical study of droplet formation under device stretching

The current work used a two-phase level-set method coupled with a laminar flow physics interface to numerically evaluate the droplet generation phenomenon in COMSOL Multiphysics 5.4 software. More details about the governing equations of the numerical modelling approach can be found in Supplementary information S-3. A flow-focusing droplet generator design was used as the geometry for the numerical analysis. The fluid properties in Table 1 were used as the material properties for the continuous and dispersed phases. Among these properties, the interfacial tension between HFE 7500 and TMPTMA was measured in one of our previous studies [55]. The fluids were considered incompressible and Newtonian. The channel boundaries were selected as wetted walls, and the contact angle (θ) was defined as π rad. Fully developed flows were initialised at the inlets as flow rates and pressure boundary condition was selected at the outlet. This simulation used shallow-channel approximation under the laminar flow physics as the fabricated microchannel height is ~137 μm. We chose 90 μL/hr as the continuous phase flow rate and 30 μL/hr as the dispersed phase flow rate to evaluate the effect of droplet generation under device stretching. A user-defined mesh was created to capture the droplet generation accurately, and a time-dependent study was used to compute the model. From Fig. 4., we can see that the droplet diameter and spacing increase with the device stretching under fixed flow conditions. In addition, droplet frequency decreased with the device stretching. We further conducted the same study with a flow rate ratio of 6:1 to validate the numerical model and included it in Supplementary information S-3. Following, we further experimentally evaluated the variation of droplet generation characteristics under different elongations obtained from the numerical analysis.

4.3. Experimental study of droplet generation under device elongation

We experimentally studied the influence of device elongation on the droplet generation properties. A continuous phase flow rate (Q_c) of 90 μL/hr and a dispersed phase flow rate (Q_d) of 30 μL/hr were chosen, which formed droplets in the dripping regime. At the initial stage (i.e., zero stretch), the generated droplets had a diameter of 88 μm ± 0.33 with a droplet spacing of 148 μm ± 1.32, Fig. 5(a). The droplets were formed at 14 Hz droplet generation frequency. As the device was stretched gradually from 0 to 5 mm by 1 mm steps, the droplet diameter increased to 102 μm ± 0.92. However, the droplet spacing showed a more complex trend of change. The droplet spacing increased when the elongation was from 0 to 3 mm, but it dropped gradually when the

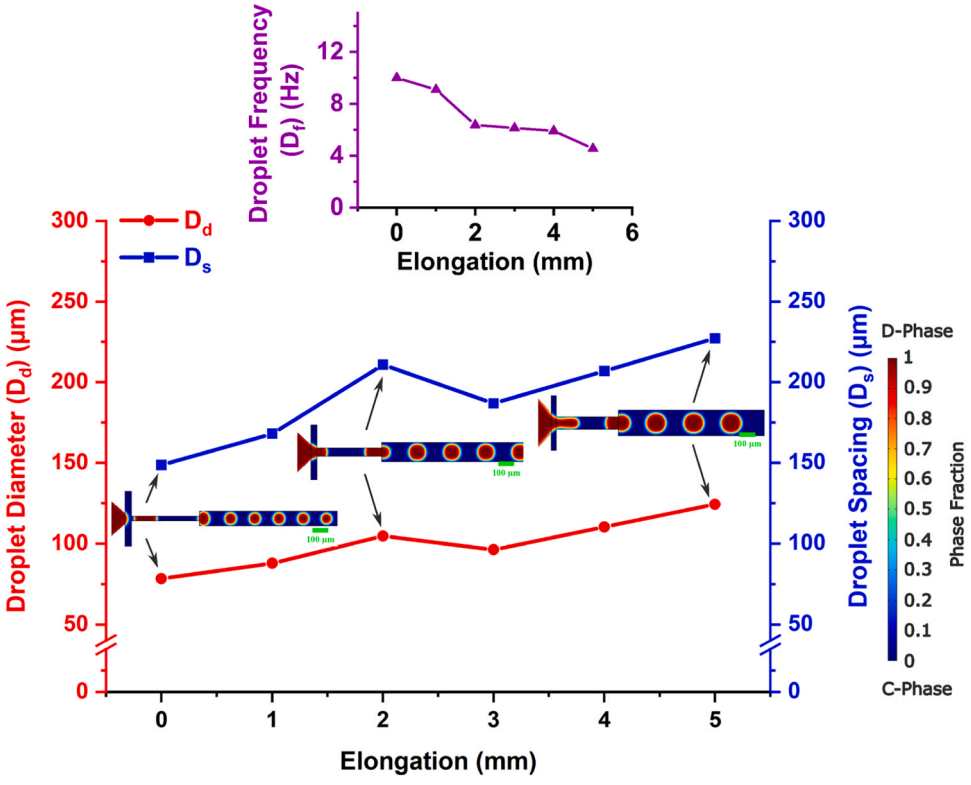

Fig. 4. Numerical studies of the influence of device lateral stretching on droplet generation characteristics such as droplet diameter (D_d), spacing (D_s) and frequency (D_f). Here, the continuous and dispersed phase flow rate ratio (Q_c/Q_d) is 3:1. Scale bars (green) of the inset images represent 100 μm.

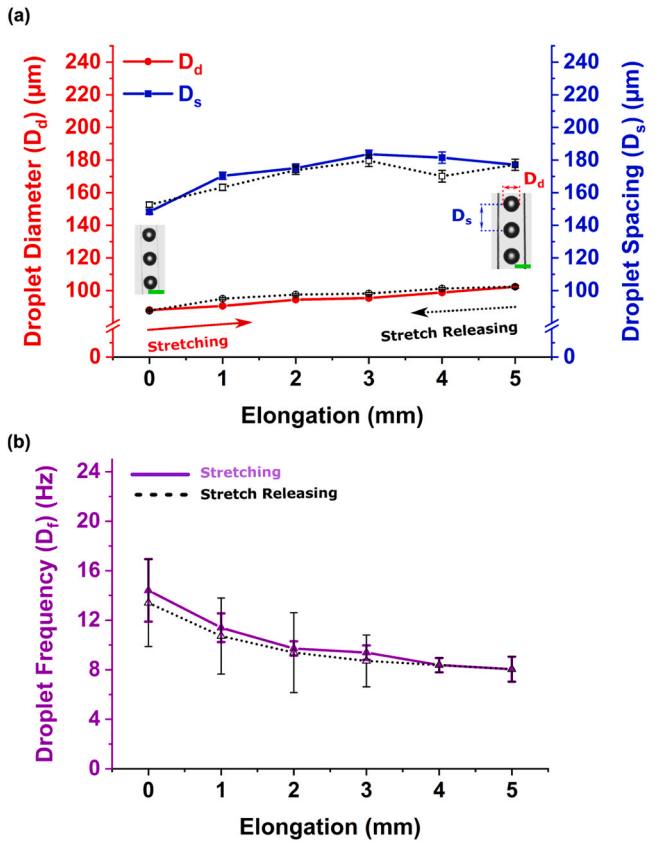

Fig. 5. Experimental study of the effect of device stretching on droplet generation characteristics under continuous and dispersed phase flow rate ratio (Q_c/Q_d) of 3:1. (a) droplet diameter (D_d), spacing (D_s). (b) droplet frequency (D_f). Each value is the average of three trials. Error bars represent the standard deviation. The scale bars (green) in the inset image represent 100 μm.

elongation exceeded 4 mm.Besides, the droplet generation frequency reduced under device elongation and reached 8 Hz at 5 mm elongation, Fig. 5(b). We also reversed the elongation from 5 mm to 0 with a 1-mm step and investigated the droplet generation characteristics. The droplet diameter and spacing were almost the same as that of the above stretching scenario, indicating negligible hysteresis. All experiments were conducted at a total flow rates below 200 μL/hr to ensure that the flexible device is free of any fluid leakages while stretching. However, optimising the settings of plasma treatment to bond flexible PDMS-PDMS membranes would allow for higher flow rates. The experimental results on the influence of device stretching on droplet generation characteristics show a similar variation obtained through the numerical simulations. However, the exact droplet diameter, spacing, and frequency values are not the same.

4.4. The effects of flow conditions on droplet generation in stretchable droplet microfluidic device

We also comprehensively studied the effects of the flow rate ratio on droplet generation properties in the stretchable microfluidic device under different elongation statuses. Fig. 6(a) shows the effect of stretching on droplet characteristics which was observed in all the flow rate conditions. We kept the total flow rate constant at 120 μL/hr while repeating the stretching experiments for different flow rate ratios.

The flow rate of the continuous phase (Q_c) varied from 100 to 60 μL/hr, and the flow rate of disperse phase (Q_d) was varied from 20 to 60 μL/hr. Fig. 6(b)-(d) show the effect of stretching the device from 0 mm to 5 mm by 1 mm steps on droplet diameter, spacing, and frequency. As shown, increasing the elongation substantially increased droplet diameter, Fig. 6(b) and droplet spacing, Fig. 6(c) while reducing the droplet frequency, Fig. 6(d). Moreover, droplet diameter reduced with increasing flow rate ratio (Q_c/Q_d) while droplet spacing increased. The droplet frequency was slightly reduced with the increase in the flow rate ratio.

In addition, we also investigated the influence of the total flow rate on droplet generation properties in the stretchable microfluidic device. We varied the flow rate of the continuous phase (Q_c) from 60 to 120 μL/hr, and the flow rate of disperse phase (Q_d) from 30 to 60 μL/hr, so that the total flow rates ranged from 90 to 180 μL/hr while the flow rate ratio (Q_c/Q_d) was constant at 2:1. Fig. 6(e) and (f) show the effect of device stretching on droplet diameter and generation frequency. We can see that increasing the device elongation substantially increased droplet diameter, Fig. 6(e) while reducing the droplet frequency, Fig. 6(f), the same as above for various flow rate ratios. Moreover, increasing the total flow rate ($Q_c + Q_d$) considerably enhances the droplet generation frequency. However, the droplet diameter dropped with increasing total flow rate.

4.5. Estimation of scaling parameters k, m, k', and m'

We can further estimate the value of parameters *k, m, k', and m'* in Eq. (6) based on the experimental data of droplet size and frequency for these stretchable droplet microfluidic devices. The data fitting for the exponential function was conducted. Fig. 7(a) shows the normalised droplet size (Eq. (6)), and Fig. 7(b) shows the pinch-off time (Eq. (9)) against the stretching variable. As observed, both results provide good fits in power laws, within 95 % confidence bounds, which describes that, by stretching the PDMS microfluidic device along the indicated direction, both droplet size and the pinch-off time increase. This also reveals that, within the current experimental data range, stretching the PDMS device has a larger influence on the geometry parameters (proportional to the droplet size) than the capillary number (inversely proportional to the droplet size), and finally causes a positive effect on the droplet size change. Additionally, k' is in the magnitude of $O\left(\frac{k}{100}\right)$ while m' is quite close to three times of m as expected. It should be noted that the determined parameters (k=2.315, m=0.235, k'=0.06153, and m' =0.7053) are only applicable for the stretchable droplet microfluidic device with flow-focusing configuration in this work. Their exact values will be different for devices of different dimensions or with varied channel configurations.

5. Conclusion

This paper reports a fully flexible and stretchable droplet microfluidic device for tunable droplet generation. The flexible droplet microfluidic device based on the flow-focusing design was developed and the device was accurately stretched along the lateral direction using a customised stretching platform. The variation of microchannel dimensions such as widths and height was evaluated by numerical modelling and experiments. The theoretical analysis, numerical modelling, and experimental characterisation were conducted to explore the influence of device lateral stretching on droplet generation characteristics. We found that the lateral stretching on the device increased the droplet diameter and spacing but reduced the droplet generation frequency. Droplet diameter and spacing increased by ~20 %, and droplet frequency decreased by ~45 % when the device was strained up to 25 %. We believe this innovative, flexible droplet microfluidic platform will provide an alternative way to precisely control the droplet formation by modifying the channel dimensions on site and in real-time without redesigning and refabricating the devices of various dimensions. This precise control of droplet generation will have broad applications for accurate single-cell encapsulation and single-cell analysis in droplets. Because flow-focusing channel arrangement enables precise control of droplet size and frequency and creates isolated

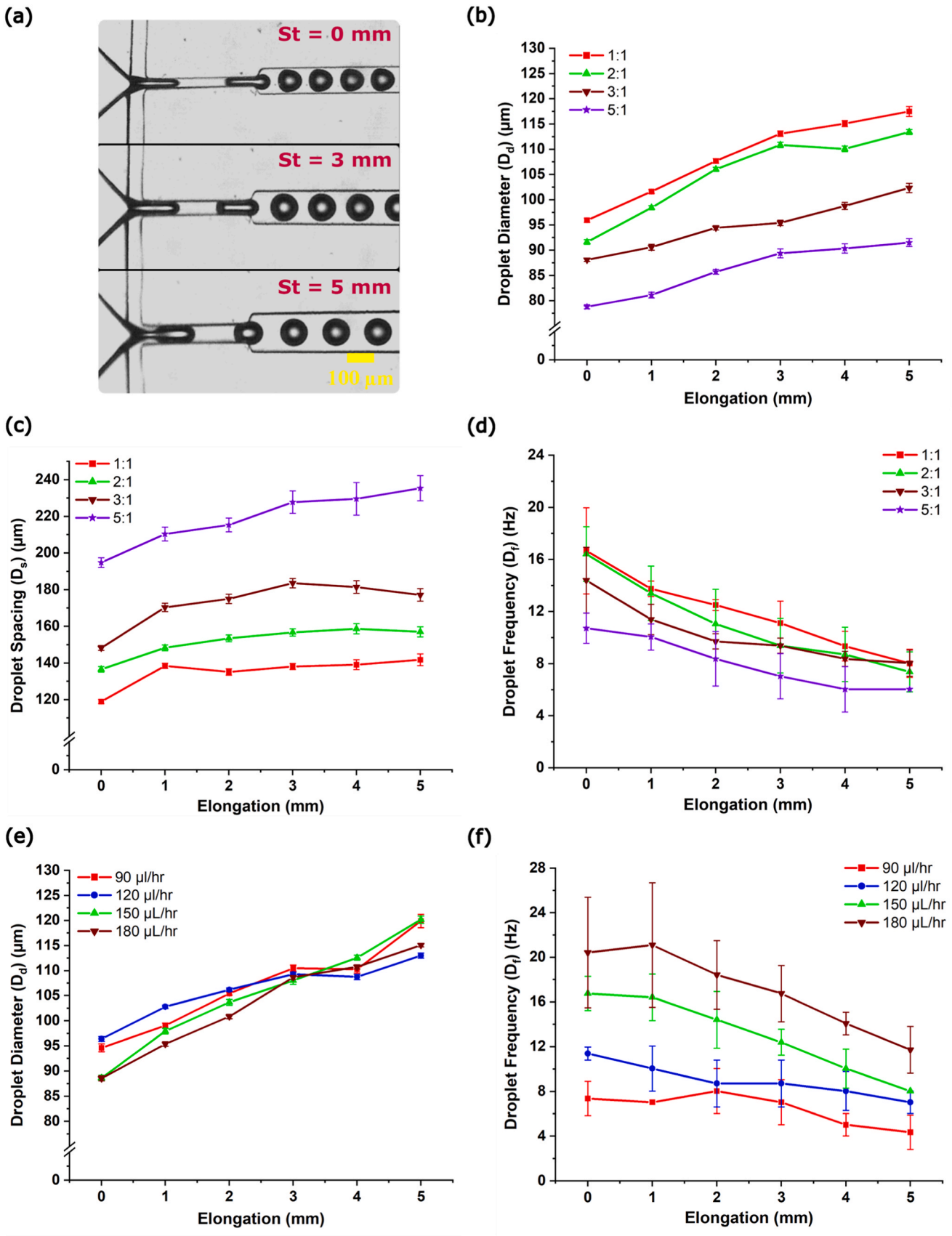

Fig. 6. Change in droplet characteristics with device elongation under different flow conditions. (a) Image of droplet generation under different elongations. (b)-(d) Droplet diameter, spacing, and generation frequency variation when changing flow rate ratios in the stretchable microfluidic device. The total flow rate is constant at 120 µL/hr. (e) and (f) Droplet diameter and generation frequency variation under the varying total flow rates. The flow rate ratio is constant at 2:1. Each value is the average of three trials. Error bars represent the standard deviation.

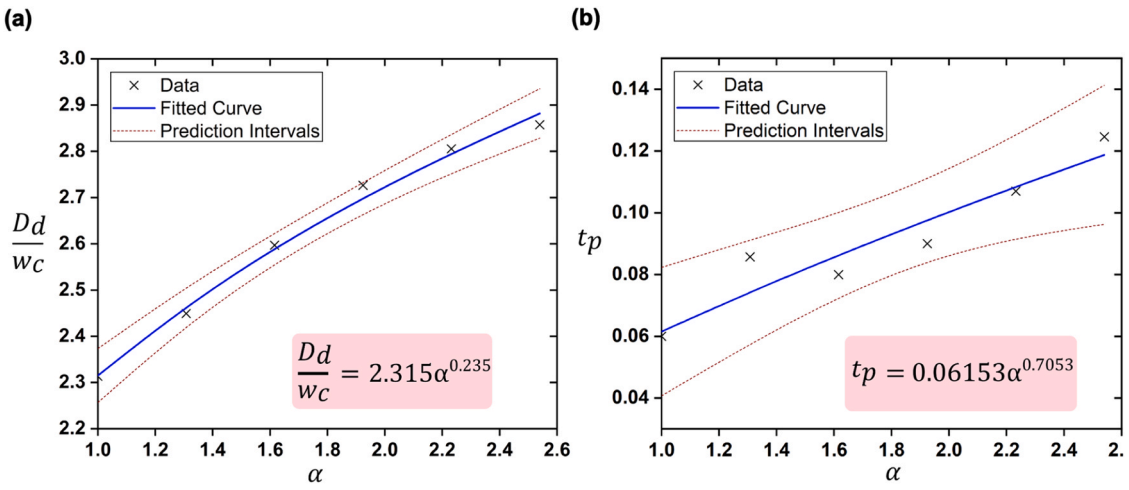

Fig. 7. Experimental data and fitted correlations in power laws: (a) Normalized droplet size against the stretching variable; (b) Droplet pinch-off time against the stretching variable.

microcompartments for analysis of individual cells. In addition, flow-focusing droplet generation with stretching minimises the shear stress on cells during encapsulation, preserving cell viability. Also, this technique allows control of the number of cells encapsulated in a particular droplet without changing the flow velocities, which could otherwise create flow instabilities by shifting between different regimes of droplet generation and affecting monodispersity.

CRediT authorship contribution statement

Nam-Trung Nguyen: Writing – review & editing, Supervision, Project administration, Funding acquisition, Conceptualization. **Amith Mudugamuwa:** Methodology, Investigation. **Jun Zhang:** Writing – review & editing, Supervision, Methodology, Data curation, Conceptualization. **Ajeet Singh Yadav:** Methodology, Investigation. **Samith Hettiarachchi:** Methodology, Investigation. **Uditha Roshan:** Writing – original draft, Visualization, Validation, Methodology, Investigation, Formal analysis, Data curation. **Yuchen Dai:** Visualization, Software.

Declaration of Competing Interest

The authors do not have any conflict of interest to declare.

Data availability

Data will be made available on request.

Acknowledgements

The authors acknowledge the support from the Australian Research Council (ARC) Australian Laureate Fellowship (Grant No. FL230100023) and ARC Future Fellowship (Grant No. FT240100020).

Appendix A. Supporting information

Supplementary data associated with this article can be found in the online version at doi:10.1016/j.snb.2024.136617.

References

[1] L. Jiang, H. Yang, W. Cheng, Z. Ni, N. Xiang, Droplet microfluidics for CTC-based liquid biopsy: a review, Analyst vol. 148 (2) (2023) 203–221.
[2] Z. Jiang, H. Shi, X. Tang, J. Qin, Recent advances in droplet microfluidics for single-cell analysis, TrAC Trends Anal. Chem. vol. 159 (2023) 116932.
[3] L. Shang, Y. Cheng, Y. Zhao, "Emerging droplet microfluidics,", Chem. Rev. vol. 117 (12) (2017) 7964–8040.
[4] S.-Y. Teh, R. Lin, L.-H. Hung, A.P. Lee, Droplet microfluidics, Lab a Chip vol. 8 (2) (2008) 198–220.
[5] T.N.D. Trinh, H.D.K. Do, N.N. Nam, T.T. Dan, K.T.L. Trinh, N.Y. Lee, Droplet-based microfluidics: applications in pharmaceuticals, Pharmaceuticals vol. 16 (7) (2023) 937.
[6] K. Schroen, et al., Droplet microfluidics for food and nutrition applications, Micromachines vol. 12 (8) (2021) 863.
[7] L. Mazutis, J. Gilbert, W.L. Ung, D.A. Weitz, A.D. Griffiths, J.A. Heyman, Single-cell analysis and sorting using droplet-based microfluidics, Nat. Protoc. vol. 8 (5) (2013) 870–891.
[8] J. Wang, et al., Droplet microfluidics for the production of microparticles and nanoparticles, Micromachines vol. 8 (1) (2017) 22.
[9] T. Moragues, S. Mitchell, D. Faust Akl, J. Pérez-Ramírez, A. deMello, Droplet-based microfluidics platform for the synthesis of single-atom heterogeneous catalysts, Small Struct. vol. 4 (4) (2023) 2200284.
[10] F. Long, et al., Recent Progress of Droplet Microfluidic Emulsification Based Synthesis of Functional Microparticles, Glob. Chall. vol. 7 (9) (2023) 2300063.
[11] O.J. Dressler, R.M. Maceiczyk, S.-I. Chang, A.J. Demello, Droplet-based microfluidics: enabling impact on drug discovery, *J. Biomol. Screen.* vol. 19 (4) (2014) 483–496.
[12] F.M. Galogahi, Y. Zhu, H. An, N.-T. Nguyen, Formation of core–shell droplets for the encapsulation of liquid contents, Microfluid. Nanofluidics vol. 25 (2021) 1–11.
[13] M. Jeyhani, R. Thevakumaran, N. Abbasi, D.K. Hwang, S.S. Tsai, Microfluidic generation of all-aqueous double and triple emulsions, Small vol. 16 (7) (2020) 1906565.
[14] A.J. Teo, et al., "Negative pressure induced droplet generation in a microfluidic flow-focusing device,", Anal. Chem. vol. 89 (8) (2017) 4387–4391.
[15] A.J. Teo, et al., Controllable droplet generation at a microfluidic T-junction using AC electric field, Microfluid. Nanofluidics vol. 24 (2020) 1–9.
[16] T. Glawdel, C. Elbuken, C.L. Ren, Droplet Generation in Microfluidics, in: D. Li (Ed.), *Encyclopedia of Microfluidics and Nanofluidics*, Springer US, Boston, MA, 2013, pp. 1–12.
[17] P. Zhu, L. Wang, Passive and active droplet generation with microfluidics: a review, Lab a Chip vol. 17 (1) (2017) 34–75.
[18] S. Svetlov, R.S. Abiev, Mathematical modeling of the droplet formation process in a microfluidic device, Chem. Eng. Sci. vol. 235 (2021) 116493.
[19] S. Marcos, R. Santos, A. Kilzer, M. Petermann, On the experimental investigation and numerical fluid dynamic simulation of LL water-in-oil dispersions in Y-junctions under the presence of dissolved CO2, J. Supercrit. Fluids vol. 146 (2019) 65–77.
[20] X.-B. Li, F.-C. Li, J.-C. Yang, H. Kinoshita, M. Oishi, M. Oshima, Study on the mechanism of droplet formation in T-junction microchannel, Chem. Eng. Sci. vol. 69 (1) (2012) 340–351.
[21] A. Sattari, P. Hanafizadeh, M.M. Keshtiban, Microfluidic preparation of double emulsions using a high aspect ratio double co-flow device, *Colloids Surf. A: Physicochemical Eng. Asp.* vol. 628 (2021) 127297.
[22] S. Hettiarachchi, et al., "Design and development of a microfluidic droplet generator with vision sensing for lab-on-a-chip devices, Sens. Actuators A: Phys. vol. 332 (2021) 113047.
[23] M. Rayner, G. Trägårdh, C. Trägårdh, P. Dejmek, Using the surface evolver to model droplet formation processes in membrane emulsification, J. Colloid Interface Sci. vol. 279 (1) (2004) 175–185.
[24] Z. Liu, C. Duan, S. Jiang, C. Zhu, Y. Ma, T. Fu, Microfluidic step emulsification techniques based on spontaneous transformation mechanism: A review, J. Ind. Eng. Chem. vol. 92 (2020) 18–40.
[25] M. Nooranidoost, R. Kumar, Geometry effects of axisymmetric flow-focusing microchannels for single cell encapsulation, Materials vol. 12 (17) (2019) 2811.

[26] B. Talebjedi, A. Abouei Mehrizi, B. Talebjedi, S.S. Mohseni, N. Tasnim, M. Hoorfar, "Machine learning-aided microdroplets breakup characteristic prediction in flow-focusing microdevices by incorporating variations of cross-flow tilt angles,", Langmuir vol. 38 (34) (2022) 10465–10477.
[27] O. Sartipzadeh, S.M. Naghib, A. Seyfoori, M. Rahmanian, F.S. Fateminia, Controllable size and form of droplets in microfluidic-assisted devices: Effects of channel geometry and fluid velocity on droplet size, Mater. Sci. Eng.: C. vol. 109 (2020) 110606.
[28] M.H. Javanmard, F. Niksirat, M.K. Moraveji, Effects of topological changes in microchannel geometries on the hydrodynamic formation and breakup of all-aqueous droplets, Phys. Fluids vol. 34 (5) (2022) 052009.
[29] S.G. Sontti, A. Atta, Regulation of droplet size and flow regime by geometrical confinement in a microfluidic flow-focusing device, Phys. Fluids vol. 35 (1) (2023) 012010.
[30] C.-H. Lee, S.-K. Hsiung, G.-B. Lee, A tunable microflow focusing device utilizing controllable moving walls and its applications for formation of micro-droplets in liquids, J. Micromech. Microeng. vol. 17 (6) (2007) 1121.
[31] F. Nalin, M.C. Tirelli, P. Garstecki, W. Postek, M. Costantini, Tuna-step: tunable parallelized step emulsification for the generation of droplets with dynamic volume control to 3D print functionally graded porous materials, Lab a Chip vol. 24 (1) (2024) 113–126.
[32] S. Yazdanparast, P. Rezai, A. Amirfazli, Microfluidic Droplet-Generation Device with Flexible Walls, Micromachines vol. 14 (9) (2023) 1770.
[33] A.R. Abate, M.B. Romanowsky, J.J. Agresti, D.A. Weitz, Valve-based flow focusing for drop formation, Appl. Phys. Lett. vol. 94 (2) (2009).
[34] H. Fallahi, J. Zhang, H.-P. Phan, N.-T. Nguyen, Flexible microfluidics: Fundamentals, recent developments, and applications, Micromachines vol. 10 (12) (2019) 830.
[35] N.-T. Nguyen, Micro elastofluidics: elasticity and flexibility for efficient microscale liquid handling vol. 11 (2020) 1004.
[36] U. Roshan, A. Mudugamuwa, H. Cha, S. Hettiarachchi, J. Zhang, N.-T. Nguyen, Actuation for flexible and stretchable microdevices, Lab a chip vol. 24 (8) (2024) 2146–2175, https://doi.org/10.1039/D3LC01086D.
[37] L. Rayleigh, On the instability of jets, Proc. Lond. Math. Soc. vol. 1 (1) (1878) 4–13.
[38] B.E. Rapp, Microfluidics: modeling, mechanics and mathematics. Elsevier, 2022.
[39] J. Sivasamy, T.-N. Wong, N.-T. Nguyen, L.T.-H. Kao, An investigation on the mechanism of droplet formation in a microfluidic T-junction, Microfluid. Nanofluidics vol. 11 (2011) 1–10.
[40] M. Mastiani, S. Seo, S.M. Jimenez, N. Petrozzi, M.M. Kim, Flow regime mapping of aqueous two-phase system droplets in flow-focusing geometries, Colloids Surf. A: Physicochem. Eng. Asp. vol. 531 (2017) 111–120.
[41] R. De Bruijn, Tipstreaming of drops in simple shear flows, Chem. Eng. Sci. vol. 48 (2) (1993) 277–284.
[42] P. Zhu, T. Kong, Z. Kang, X. Tian, L. Wang, Tip-multi-breaking in capillary microfluidic devices, Sci. Rep. vol. 5 (1) (2015) 11102.
[43] L. Wu, X. Liu, Y. Zhao, Y. Chen, Role of local geometry on droplet formation in axisymmetric microfluidics, Chem. Eng. Sci. vol. 163 (2017) 56–67.
[44] P. Garstecki, M.J. Fuerstman, H.A. Stone, G.M. Whitesides, Formation of droplets and bubbles in a microfluidic T-junction—scaling and mechanism of break-up, Lab a Chip vol. 6 (3) (2006) 437–446.
[45] A. Gupta, R. Kumar, Effect of geometry on droplet formation in the squeezing regime in a microfluidic T-junction, Microfluid. Nanofluidics vol. 8 (6) (2010) 799–812.
[46] H. Liu, Y. Zhang, Droplet formation in microfluidic cross-junctions, Phys. Fluids vol. 23 (8) (2011) 082101.
[47] A. Müller, M.C. Wapler, U. Wallrabe, A quick and accurate method to determine the Poisson's ratio and the coefficient of thermal expansion of PDMS, Soft Matter vol. 15 (4) (2019) 779–784.
[48] A.J. Teo, F. Malekpour-galogahi, K.R. Sreejith, T. Takei, N.-T. Nguyen, Surfactant-free, UV-curable core–shell microcapsules in a hydrophilic PDMS microfluidic device, Aip Adv. vol. 10 (6) (2020) 065101.
[49] P. Kim, K.W. Kwon, M.C. Park, S.H. Lee, S.M. Kim, K.Y. Suh, Soft lithography for microfluidics: a review, BioChip vol. 2 (1) (March 2008 2008) 1–11.
[50] H. Fallahi, S. Yadav, H.-P. Phan, H. Ta, J. Zhang, N.-T. Nguyen, "Size-tuneable isolation of cancer cells using stretchable inertial microfluidics,", Lab a Chip vol. 21 (10) (2021) 2008–2018.
[51] H. Fallahi, et al., On-demand deterministic release of particles and cells using stretchable microfluidics, Nanoscale Horiz. vol. 7 (4) (2022) 414–424.
[52] H. Fallahi, J. Zhang, J. Nicholls, H.-P. Phan, N.-T. Nguyen, "Stretchable inertial microfluidic device for tunable particle separation,", Anal. Chem. vol. 92 (18) (2020) 12473–12480.
[53] A. Lashkaripour, D.P. McIntyre, S.G. Calhoun, K. Krauth, D.M. Densmore, P. M. Fordyce, Design automation of microfluidic single and double emulsion droplets with machine learning, Nat. Commun. vol. 15 (1) (2024) 83.
[54] K. Matsumoto, S. Sogabe, T. Endo, Synthesis and properties of methacrylate-based networked polymers having ionic liquid structures, J. Polym. Sci. Part A: Polym. Chem. vol. 48 (20) (2010) 4515–4521.
[55] Y. Dai, et al., Dynamic behaviours of monodisperse double emulsion formation in a tri-axial capillary device, Micromachines vol. 13 (11) (2022) 1877.
[56] A.S. Basu, "Droplet morphometry and velocimetry (DMV): a video processing software for time-resolved, label-free tracking of droplet parameters,", Lab a Chip vol. 13 (10) (2013) 1892–1901.
[57] I.D. Johnston, D.K. McCluskey, C.K. Tan, M.C. Tracey, Mechanical characterization of bulk Sylgard 184 for microfluidics and microengineering, J. Micromech. Microeng. vol. 24 (3) (2014) 035017.

Uditha Roshan received his Bachelor of the Science of Engineering Honours and the Master of Philosophy degrees in Mechanical Engineering from the University of Moratuwa, Sri Lanka in 2016 and 2022 respectively. He started his doctoral studies in 2023 and is currently a Ph.D. candidate at Queensland Micro- and Nanotechnology Centre (QMNC), Griffith University, Australia. His research focuses on design and development of microelastofluidic systems for biomedical applications. His research interests are microfluidics, microelastofluidics, smart material-based actuation, and micro/nano-electromechanical systems (MEMS/NEMS).

Yuchen Dai completed his Ph.D. at the University of Queensland (UQ), Australia, in 2021. From 2021–2023, he was a research fellow at Queensland Micro Nanotechnology Centre (QMNC) at Griffith University. After that, he joined Australian Institute of Bioengineering and Nanotechnology, and school of Chemical engineering at the University of Queensland as a postdoctoral research fellow. His research interests include plume theory, boundary layer theory, multiphase flow, computational fluid dynamics (CFD) modelling, microfluidic technology.

Ajeet Singh Yadav is a researcher in the field of digital microfluidics and currently pursuing his Doctor of Philosophy at the Queensland Micro- and Nanotechnology Centre (QMNC), Griffith University in Australia. His academic journey began with a bachelor's degree in production engineering from the National Institute of Technology, Agartala, India in 2016, followed by a master's degree in Nanotechnology from the National Institute of Technology, Calicut, India in 2019. Ajeet's research focuses on the fabrication and analysis of digital microfluidic platforms, such as liquid marbles and liquid beads, with applications in biotechnology. He is also engaged in the development of image-processing strategies tailored for digital PCR and protein array analysis.

Samith Hettiarachchi received his honours degree in engineering (mechanical engineering) from the University of Moratuwa, Sri Lanka. He is currently a Ph.D candidate at Queensland Micro- and Nanotechnology Centre (QMNC), Griffith University, Australia. His research focuses on developing mechanisms for submicron to nanoparticle manipulation, focusing, and separation using microfluidics. His research interests are microfluidics, lab-on-a-chip, inertial microfluidics, viscoelastic microfluidics and computational fluid dynamics.

Amith Mudugamuwa received his bachelor's degree in mechanical engineering from the University of Moratuwa (UOM), Sri Lanka in 2017. He received his MPhil. in mechatronic engineering from Shandong University of Science and Technology (SDUST), China in 2020. He is currently a PhD candidate in candidate at Queensland Micro- and Nanotechnology Centre (QMNC), Griffith University, Australia. His current research focuses on innovative inertial microfluidics for micro/nano particle manipulation. His research interests include microfluidics, lab-on-a-chip, micro/nano-electromechanical systems (MEMS/NEMS), computer vision, vibration-based sensing, and artificial intelligence.

Jun Zhang is a Senior Lecturer at the School of Engineering and Built Environment, Griffith University, Australia. He was a recipient of an ARC DECRA fellowship (2021–23). He received his bachelor's degree in engineering with an Outstanding Graduate Award from the Nanjing University of Science and Technology (NUST), China, in 2009, and received a PhD degree in Mechanical Engineering from the University of Wollongong, Australia, in 2015. His research is to explore the passive fluid dynamics, active external (electrical, acoustic, magnetic etc.) force fields and their combination to accurately manipulate micro- and nanoparticles in rigid and flexible microfluidic platforms, as well as develop microfluidic technologies for disease diagnosis and therapeutics.

Nam-Trung Nguyen is an Australian Laureate Fellow. He received his Dipl-Ing, Dr Ing, and Dr Ing Habil degrees from Chemnitz University of Technology, Germany, in 1993, 1997, and 2004, respectively. From 1999–2013, he was an Associate Professor at Nanyang Technological University in Singapore. Since 2013, he has served as a Professor and the Director of Queensland Micro- and Nanotechnology Centre of Griffith University, Australia. He is a Fellow of ASME and a Senior Member of IEEE. His research is focused on microfluidics, nanofluidics, micro/nanomachining technologies, micro/nanoscale science, and instrumentation for biomedical applications. One of his current research interests is developing flexible and stretchable systems with bio interface.